Effect on albumin and fibronectin adsorption of silver doping via ionic exchange of a silica-based bioactive glass

Ceramics International xxx (xxxx) xxx

Contents lists available at ScienceDirect

Ceramics International

journal homepage: www.elsevier.com/locate/ceramint

Effect on albumin and fibronectin adsorption of silver doping via ionic exchange of a silica-based bioactive glass

Jacopo Barberi [a,*], Luisa Mandrile [b], Andrea M. Giovannozzi [b], Marta Miola [a], Lucia Napione [a], Andrea M. Rossi [b], Alessandra Vitale [a], Seiji Yamaguchi [c], Silvia Spriano [a]

[a] DISAT Department, Politecnico di Torino, Corso Duca degli Abruzzi 24, 10129, Torino, Italy
[b] Chemical Physics and Nanotechnology department, National Institute of Metrological Research, Strada delle Cacce 91, 10137, Torino, Italy
[c] Department of Biomedical Sciences, College of Life and Health Sciences, Chubu University, 1200 Matsumoto, Kasugai, Aichi, 487-8501, Japan

ARTICLE INFO

Handling Editor: P. Vincenzini

Keywords:
Protein adsorption
Bioactive glass
Silver
Ionic exchange
Surface characterization

ABSTRACT

Protein adsorption is a crucial step in the life of biomaterials for bone application, such as bioactive glasses. The investigation of adsorption mechanisms is a difficult task per se, which is even more complex on bioactive glasses due to surface reactivity. Here, the effect of silver doping by ionic exchange on the interaction of a silica-based bioactive glass with albumin and fibronectin, serum proteins related to osseointegration, is reported. The presence of silver does not change relevant surface properties such as topography, surface energy, wettability, or surface ζ potential. Nevertheless, the interactions with proteins are much different. The presence of silver significantly increases the adsorption of albumin and fibronectin and leads to a higher loss of secondary structure compared to the undoped surface, as a consequence of the interactions and bonding between silver and thiols in the cysteine residues. Selectivity of silver-doped glass is discovered: Ag enhances more adsorption and denaturation of albumin since it has more cysteines than fibronectin. It is also here observed that due to the formation of a hydrated silica gel layer during adsorption, proteins are not only present on the surface of the bioactive glasses, but also embedded inside the surface reaction layer.

1. Introduction

Bone infections in implantation sites have a statistical impact of about 1–2% [1] and the complete removal of the infected area is particularly challenging, involving massive antibiotic usage, hospital stays, eventual revision surgeries, and implant replacement, with related high social and economic costs [2]. Antibiotics have drastically improved our life, nevertheless, a new threat is arising due to their abuse and misuse, coupled with the evolution of antimicrobial resistance [3]. The ineffectiveness of antibiotics is predicted to result in 10 million annual global deaths by 2050 [4]. Biomaterial scientists and engineers have joined the efforts to fight the risk of peri-implant infections and to reduce the use of antibiotics by developing intrinsic antibacterial materials: a special focus is on biomaterials for bone tissue repair. Several strategies have been developed to confer antibacterial and antifouling properties to different implantable materials, moving from loading or coating the material with antibiotics, such as antibiotic-loaded polymethylmethacrylate bone cement [2,5], to grafting bactericidal ions or molecules [6] or modifying wettability, surface charge, and topography to reduce bacterial adhesion [7–9]. Antibacterial metals [10] can be directly implanted on the surface as ions (mainly Ag^{+}, Cu^{2+}, and Zn^{2+} [11]) or nanoparticles (NPs) [12] or embedded within bioactive materials, such as hydroxyapatite [2]. Interestingly, it is quite easy to incorporate biologically active ions into bioactive glasses (BGs). The ease of changing the glass composition and the virtually unlimited combinations have led material scientists to incorporate many different elements within the glass, such as Ag, Mg, Sr, Zn, F, and Zr [13]. Those ions can be incorporated into the glass composition or introduced only onto the surface by ionic exchange [14]. In both cases, it is possible to confer antibacterial capability to bioactive glasses for tissue regeneration [15]. When antibacterial ions are introduced in the glass structure as modifier oxide it may change the glass properties, such as crystallization, characteristic temperatures [16] and dissolution [13]. The ionic exchange process allows for maintaining unchanged the bulk properties, which can be designed according to the desired application while conferring new properties just to the glass surface. Furthermore, a more

* Corresponding author.
E-mail address: jacopo.barberi@polito.it (J. Barberi).

https://doi.org/10.1016/j.ceramint.2022.12.251
Received 24 August 2022; Received in revised form 20 December 2022; Accepted 26 December 2022
Available online 28 December 2022

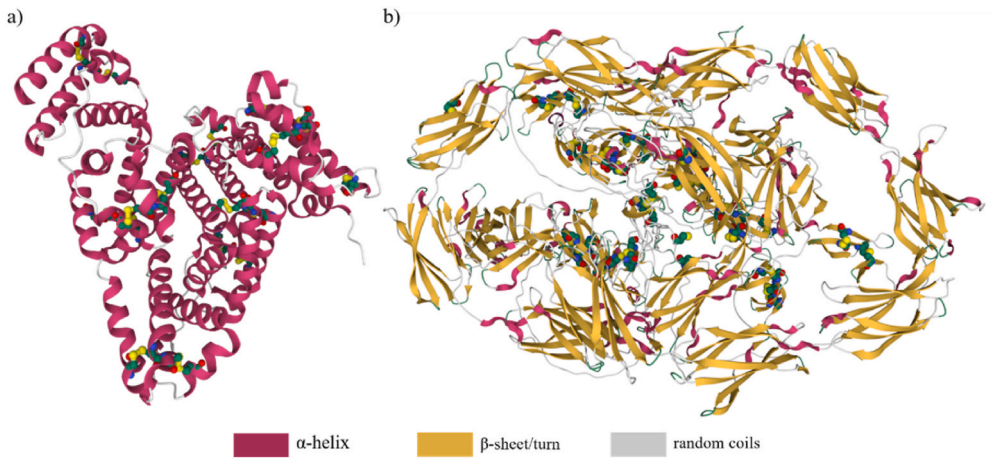

Fig. 1. 3D representation of the structure of bovine serum albumin (a)(PBD entry 4F5S, https://doi.org/10.2210/pdb4f5s/pdb [35]) and the predicted structure of a fibronectin subunit (b)(UniProt entry P07589·FINC_BOVIN [36]). Cysteine residues are highlighted using a ball-stick representation. The positions of the disulphide bridges are reported in the supporting information.

homogeneous distribution of silver can be obtained by ionic exchange with respect to use of silver as a precursor [17].

Besides reducing the risk of infection, biomaterials for bone substitution and regeneration shall induce an appropriate response by the host to achieve proper osseointegration and implant success. This process does not involve only osteogenic cells, such as osteoblasts, but also a complex interplay between the skeletal and immune systems (osteoimmunomodulation) [18]. Plasma proteins and molecules are immediately adsorbed on the implant surface, forming a transient matrix that can evolve, according to the Vroman effect [19]. Then, acute inflammation is the first part of the foreign body reaction (FBR) and it involves the migration of polymorphonuclear leukocytes or neutrophils to the damaged sites [20]. Activated neutrophils attempt to degrade the biomaterials and produce chemo-attractants and cytokines to recruit monocytes [21]. Monocytes further differentiate into macrophages, starting the chronic inflammation and forming foreign body giant cells with the consequent fibrous capsule formation: this phenomenon avoids the biomaterial osseointegration [20]. On the other hand, they have an active role in the bone formation process, which can be both osteogenic or osteolytic according to the different polarizations [18].

Among the factors that control the cellular response to an implant, there is the protein transitional matrix. Adsorbed proteins have an active role in cell adhesion, activation, and also in FBR course [22]. For example, some proteins, such as fibronectin (FN) and vitronectin, are well-recognized to enhance cell adhesion [23]. Albumin can exert an anti-inflammatory effect thanks to its radical-scavenging activity and reduction in macrophage adhesion [24], increases osteogenesis by sustaining mesenchymal stem cell proliferation [25], and reduces bacteria adhesion [26]. The adsorption of protein from blood and biological fluids is a very complex process that depends upon a variety of different factors, including various surface properties, the composition of the protein solution, its ionic strength, pH, and temperature. According to these factors, proteins can interact with the surface through hydrophobic interactions, electrostatic or hydrogen bonding. They can have a different affinity towards different surfaces and bind in a more loosely or strong manner, even by partially losing their secondary and tertiary structures [27]. Among the various medical materials that have been widely investigated concerning protein adsorption (steel [28], bioceramics [29], and titanium [27]), bioactive glasses are one of the more complex. As recently reviewed by Zheng et al. [30], the extremely high reactivity of BGs in physiological conditions drastically influences the adsorption process, increasing also the difficulty of its characterization. Within the different BG properties, such as composition, degree of crystallinity, and surface topography, the presence of doping elements, as in the case of bioactive metal ions, significantly changes protein-material interactions. The influence of silver ions within a BG on protein adsorption has been scarcely investigated. silver was incorporated in the bulk of both melt- [31] or sol-gel derived silica glasses [32,33] and the presence of silver, both in the ionic (Ag^{+}) or metallic (Ag^{0}) forms, is expected to increase the adsorption of proteins, such as hemoglobin [34] or bovine serum albumin (BSA) [31], proportionally to the silver content. The interaction between Ag and the thiol groups in the cysteine (Cys) residues (Fig. 1) of proteins was found to be strong, leading even to the rupture of disulphide bridges, and to be responsible for partial protein denaturation [31].

In this work, the effects of silver doping on the surface of a melt-derived silica-based bioactive glass on the interactions with the proteins relevant for osteoimmunomodulation, such as albumin and fibronectin, are investigated. Protein solutions close to the physiological concentration are used in this work to mimic the physiological environment. After a deep characterization of the surface properties of the glasses, the adsorbed protein layers are characterized in terms of protein amount, distribution, and conformation, merging traditional techniques, such as mid-infrared spectroscopy or fluorescent labeling, with some innovative ones, such as Kelvin probe force microscopy (KPFM) and zeta potential titration. The use of this set of characterization techniques allowed to get new information about the adsorption of BSA and fibronectin (FN). The results are compared with the literature on protein adsorption on BGs considering that the distinctive feature of the BG used in this research is the presence of silver only in a surface layer [31–34,37–41]. Furthermore, FN adsorption on silver-containing BGs has never been reported before to the best of the authors' knowledge.

2. Materials and Methods

2.1. Sample preparation

Glass disks (1 cm in diameter) were prepared by melting and casting. Briefly, the precursors of the bioactive glass SBA2 (composition, mol%: 48% SiO_2, 18% Na_2O, 30% CaO, 3% P_2O_5, 0.43% B_2O_3, 0.57% Al_2O_3; Sigma Aldrich, St. Louis, USA) [42] were melted at 1450 °C for 1 h in a platinum crucible, then cast in a cylindrical brass mold (1 cm diameter), preheated at 500 °C, and annealed at 500 °C for 14 h. The bar was then cut for obtaining 2 mm thick disks, which were subsequently gritted with SiC abrasive papers (up to 1000 grit) and washed with Milli-Q water in an ultrasound bath for 10 min twice. Henceforth, these samples will be referred to as SBA2. Antibacterial ability was conferred to the glass via an ionic-exchange process by soaking SBA2 samples in a

0.03 M $AgNO_3$ (Sigma Aldrich, St. Louis, USA) aqueous solution for 1 h at 37 °C, in an orbital shaker (100 rpm) [43]: at the end of the process, samples were gently washed in bi-distilled water and dried at room temperature. These samples will be referred to as AgSBA2. Samples were stored in air and dark condition.

2.2. Biological reagents

Unlabeled BSA and FN were obtained by Sigma Aldrich (St. Louis, USA). Commercially available fluorescent proteins were purchased: tetramethylrhodamine-conjugated BSA was obtained by Invitrogen (Waltham, USA) and rhodamine-conjugated FN by Cytoskeleton Inc. (Denver, USA).

2.3. Protein adsorption

To mimic the physiological environment as much as possible, the BSA and FN solutions were prepared in phosphate-buffered saline (PBS) solution at pH 7.4, with a concentration of 20 mg/ml and 0.2 mg/ml respectively, which are reported to be their concentration in plasma [44]. BSA adsorption was carried out by soaking the samples in 1 ml of solution in a multiwell, while FN was adsorbed by covering the surface with 125 µl of solution and placing the glass disks in a moisturized chamber to avoid water evaporation. The samples were placed in an incubator at 37 °C for 2 h, as previously reported [44]. Then, the specimens were gently rinsed with milli-Q water to remove loosely bound proteins, dried under a biological hood, and stored at 4 °C until use. Samples with BSA will be labeled as SBA2_BSA and AgSBA2_BSA, and samples with FN as SBA2_FN and AgSBA2_FN.

The adsorption protocol was optimized for KPFM and fluorescent measurements since these two techniques have strict and very specific needs. To assess the presence of the protein layer by KPFM, a contrast in the potential images is necessary. Therefore, the glass disks were partially covered with a drop of protein solution, incubated in a moisturized chamber and washed as described above. For fluorescent experiments, a small drop of fluorophore-conjugated protein solution (10 µl) was deposited on sample surfaces and then covered by a microscope cover glass, in order to ensure complete coverage of the surface by a protein film and avoid water evaporation. Again, samples were incubated in a moisturized chamber at 37 °C for 2 h and gently rinsed trice in PBS and trice in milli-Q water. A more thorough washing was needed to avoid fluorescent signal interferences. For fluorescent quantification and imaging, the samples were prepared using an aqueous mounting medium (Fluoroshield; Sigma Aldrich, St. Louis, USA) and analyses were performed within the day.

2.4. Substrate characterization

The topographical and surface properties of SBA2 and Ag-SBA2 were analyzed through profilometry, wettability and surface energy measurements. Surface 3D images were obtained using a laser optical profilometer (50× objective, LSM 900, ZEISS, Oberkochen, Germany) and surface roughness parameters were measured from surface reconstruction, obtained with a 20× objective, according to ISO 25178, using the Confomap software. The measurements were performed on three different samples and data are reported as average ± standard deviation (SD).

The static contact angle was measured with the sessile drop technique (FTA 1000C, First Ten Angstrom, Portsmouths USA) with two different liquids, water and hexadecane, with a respective surface tension of 72.1 mN m^{-1} and 28.1 mN m^{-1}. Three different samples were measured with each liquid and the overall surface energy, the polar and the dispersive components were calculated by the Owens-Wendt method [45] and data are reported as average ± standard deviation (SD).

2.5. Zeta potential titration curves

Zeta potential titration curves were acquired for BSA and FN in solution and for bioactive glass surfaces before and after the adsorption of the proteins. Dynamic light scattering (DLS - Litesizer 500, Anton Paar, Gratz, Austria) was employed to analyze the protein solutions. BSA and FN were dissolved in PBS at an initial concentration of 35 mg/ml and 0.2 mg/ml respectively, followed by aliquoting with KCl 1 mM in order to reach a final concentration of 5 mg/ml for BSA and 0.01 mg/ml for FN. 0.05 M HCl and 0.05 M NaOH were used to titrate the protein solutions to the following pH values: 2.5, 3, 3.5, 4, 5, 6, 7, 8, 9. SBA2 and AgSBA2 disks were analyzed using an electrokinetic analyzer (SurPASS, Anton Paar, Gratz, Austria) equipped with an adjustable gap cell and an automatic titration unit. KCl 0.001 M was used as electrolyte and 0.05 M NaOH and 0.05 M HCl as titration solution. Fifteen points have been measured for both the basic and the acidic range. For each range, a couple of different samples were used due to the possibility of surface modification during the measurement.

2.6. X-ray photoelectron spectroscopy

Surface chemistry before and after protein adsorption was determined by XPS measurements (XPS, PHI 5000 Versaprobe II, ULVAC-PHI, Inc., Kanagawa, Japan). The X-rays were generated by an Al–K source and the take-off angle was 45°. Survey spectra were recorded to determine the elemental composition, while high-resolution spectra in the C1s and N1s regions were acquired with a pass energy of 0.1 eV. Peaks were deconvoluted by the CasaXPS software. Before deconvolution, the spectra were calibrated by setting the C1s peak, referred to the C–C bonds, at 284.8 ± 0.1 eV [46]. A Shirley background function was used for the C1s peaks while a linear function was used for the N1s peaks. The peaks were fitted by Gaussian-Lorentzian (70-30%) curves, allowing a shift of ±0.2 eV and constraining the full width at half-maximum between 1.1 and 1.6 eV [47]. The XPS analyses were performed on the as-prepared samples, after adsorption of the proteins and on some samples which were subjected to the acidic titration range during the zeta potential analysis. These last samples will be referred to as SBA2z, SBA2_BSAz, SBA2_FNz, AgSAB2z, AgSBA2_BSAz, and AgSBA2_FNz.

2.7. Protein quantification

Two different methods were employed to quantify the proteins adsorbed on the bioactive glasses. At first, the bicinchoninic acid (BCA) assay (Thermofisher, Waltham, USA) was exploited. This test is based on the colorimetric reaction between two molecules of bicinchoninic acid and a copper ion, reduced by proteins from Cu^{+2} to Cu^{+1}, which develop a purple color. Protein in solution can be quantified by measuring the adsorbance of the reacted medium at 562 nm and comparing the results with an appropriate calibration curve. In order to ensure a correct quantification, the measured amount shall be included within the extremes of the calibration curves. According to the literature, very few micrograms of proteins are expected to adsorb on a surface [38,39], which fall below the lowest concentration suggested by the manufacturer for the standard BSA curves, 25 µg/ml. Therefore, a new standard curve was obtained, setting the concentration range from 0 to 10 µg/ml (Fig. S1). Since different proteins might reduce a different amount of copper ions per protein molecule, the calibration curve shall be measured using the protein of interest. As consequence, FN was not quantified by BCA because it was not possible to perform the calibration with FN due to the limited availability of the protein itself. This test was performed only on BSA. Briefly, the samples with adsorbed BSA were placed in a 24-multiwell and soaked in 300 µl of 2% SDS (Bioreagent Thermofisher, Waltham, USA) for 2 h to detach the adsorbed proteins [48]. On the other hand, both proteins were quantified by fluorescence. SBA2_BSA, SBA2_FN, AgSBA2_BSA, and AgSBA2_FN samples were prepared as described above, and then the fluorescent emission of

rhodamine-conjugated BSA and FN was measured with a ChemiDoc MP system (Bio-Rad) using the Rhodamine application (excitation source: green epi-illumination; emission filter: 602/50 nm). Samples with BSA and FN, along with SBA2 and Ag-SBA2 samples without proteins were analyzed in separate acquisitions. Data are reported after the removal of the background signal of SBA2 and AgSBA2 without proteins.

2.8. Kelvin probe force microscopy

KPFM measurements were performed by acquiring the topographical image during the forward scan in tapping mode and the potential image during the backward scan in lift mode (Innova atomic force microscope, Bruker, Billerica, USA). Conductive Sb-doped tips with a nominal frequency of 75 kHz were used (SCM-PIT-V2, Bruker, Billerica, USA). Measuring parameters (scanning rate, lift height, KPFM parameters) were adjusted each time in order to achieve optimal experimental conditions. Topographical and surface potential images (100 × 100 μm) were obtained in the area of the border of the drop for simultaneously visualizing the protein layer and bare substrate. Images were elaborated by using the Gwyddion software [49]. The topographical images were processed by a two-degree polynomial function while the lines in the surface potential images were aligned using the matching function of the software.

2.9. Fluorescent imaging

Fluorescent images of the samples after adsorption were acquired by fluorescent optical microscopy (LSM 900, ZEISS, Oberkochen, Germany - emission wavelength: 540–562 nm). The scope of this analysis was to observe the coverage and distribution of the proteins on the surfaces, not to quantify and compare the signal intensity on different samples, which was done as previously described. Therefore, color gamma has been post-processed to obtain the best visual results.

2.10. Attenuated total reflectance infrared spectroscopy

ATR-FTIR spectra were acquired with an FT-IR spectrometer (Nicolet iN10 Infrared Microscope, Thermo Fischer Scientific, Waltham, USA) equipped with a Se/Ge ATR tip. The cooled MCT detector was selected to collect the spectra in the range 1000–4000 cm^{-1} with a resolution of 4 cm^{-1} with 64 accumulation for each spectrum. The spectral background was acquired with the ATR tip in the air before every measurement. Spectra were collected on three different points of the samples and averaged before plotting. The Amide I band region, in the range of 1700-1600 cm^{-1}, was deconvoluted to investigate the secondary structure of the adsorbed proteins. Baseline correction was performed employing a linear function and the band deconvolution was handled by the Thermo Scientific Peak Resolve tool in the OMNIC software. The Savitsky-Golay second derivative method for the minima identification was performed and peak shapes were modeled with a Voigt shape. Reference spectra were collected for native BSA and FN and after thermal denaturation at 100 °C for 1 h (BSA_h and FN_h). Denaturation was achieved by heating proteins on a microscope glass in an oven. The spectra were used to confirm the changes in the Amide I band after the loss of the native protein structure and the feasibility of secondary structure analysis with the experimental set-up used in this work.

3. Results and discussion

3.1. Effect of silver doping on the surface properties

The formation of a protein layer on biomaterials is strictly related to the properties of the surface, such as roughness, functional groups, chemical composition, surface charge, and energy [50]. Due to the complexity of this phenomenon, the role of each single surface property on the mechanisms of protein adsorption is still under investigation [30]. Therefore, the detailed surface characterization of SBA2 and AgSBA2 samples, which was carried out in this paper, is fundamental to understanding the effect of Ag doping on protein adsorption on a bioactive glass surface.

Table 1
XPS elemental composition of SBA2 and AgSBA2.

	Atomic Composition (%)							
	Si	O	C	Ca	Ag	P	Na	N
SBA2	5.03	34.35	46.35	7.61	–	–	2.85	–
AgSBA2	11.70	40.88	33.63	2.84	6.88	1.49	2.88	0.71

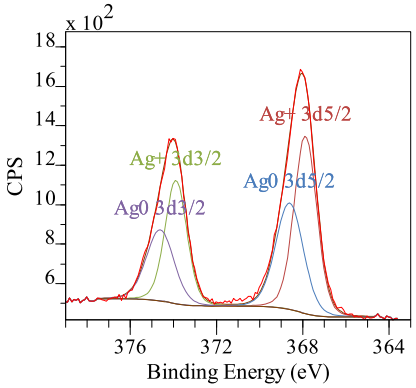

Fig. 2. Deconvolution of the Ag3d region for AgSBA2.

At first, the surface chemistry was investigated to assess the presence of Ag within the glass surface. XPS atomic quantification is reported in Table 1. Many of the elements expected from the glass composition have been found along with a high content of C, which derives from random environmental contamination. Other elements of the glass composition, such as Al or P in the case of SBA2, might be too low in concentration to be detected, also due to the presence of contaminants. B cannot be correctly quantified by XPS, as previously reported [46], and it is not included. C% is higher on SBA2, accounting for the lower content of Si and O. As it is possible to observe from the Ca/Si and Na/Si ratio, respectively decreasing from 1.5 to 0.2 and from 0.6 to 0.2, the amount of Ca^{2+} and Na^{+} is reduced after the ionic exchange treatments, since those ions are involved in the exchange process, as previously reported by the authors [43,51]. As expected, Ag was found only on the treated surface, confirming that the ion-exchange process is effective to dope the glass surface. The presence of N in this sample may be a residual from the ion exchange process.

The presence of both metallic (Ag^0) and ionic (Ag^+) Ag was observed by deconvolution of the Ag3d region, with the typical 3d3/2 3d5/2 split, reported in Fig. 2. The binding energy for metallic silver in the 3d5/2 peak is about 368.4 eV, while for ionic silver it is 367.9 eV. The energy split between 3d5/2 and 3d3/2 peaks is 6 eV [52,53]. According to the area of the different components, Ag is present mainly as an ion (Ag^+). The elemental state of Ag (Ag^0) has previously been reported to affect protein adsorption on BGs: metallic Ag (Ag^0) enhances the interaction of proteins with the surface and provokes more unfolding with respect to its ionic form (Ag^+) [31].

The topography of the samples was evaluated using a laser confocal profilometer. As observable in the 3D reconstruction of the surface (Fig. 3 a and b), the morphology of both samples is very similar and characterized by the grooves typical of the polishing process. The surface roughness parameters, such as arithmetic average (S_a), root mean square (S_q), Skewness (S_{sk}), and Kurtosis (S_{ku}), are reported in Table 2. The S_a and S_q values are quite similar and low for both surfaces, as expected for polished samples, with little higher values for AgSBA2. The

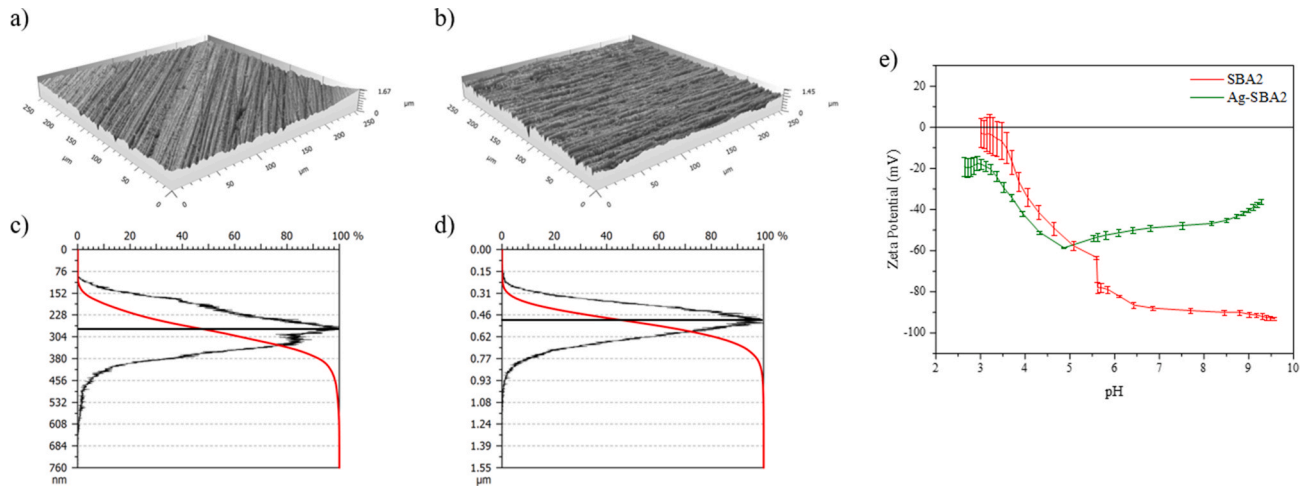

Fig. 3. 3D surface reconstruction of SBA2 (a) and AgSBA2 (b) surfaces. The plot of the amplitude distribution function (black) and the Abbot-Firestone curve (red) vs depth from the highest surface point for SBA2 (c) and AgSBA2 (d). The surface average line is represented by the black horizontal line. Solid surface zeta potential vs pH titration curves of the undoped and doped glass samples (e). (For interpretation of the references to color in this figure legend, the reader is referred to the Web version of this article.)

Table 2
Topographical parameters (arithmetic average roughness, Sa; root mean square roughness, Sq; Skewness, Ssk; Kurtosis, Sku), wettability (water contact angle, θ) and surface energy (dispersive component, γd; polar component, γp) of SBA2 and AgSBA2. All values are expressed as average ± standard deviation.

	Topographical Parameters				Wettability & Surface Energy		
	S_a (nm)	S_q (nm)	S_{sk}	S_{ku}	θ (°)	γ^d (mN/m)	γ^p (mN/m)
SBA2	51.8 ± 10.1	65.8 ± 13.5	−0.51 ± 0.14	3.67 ± 0.65	22.0 ± 2.6	26.51 ± 0.13	41.69 ± 0.99
AgSBA2	70.9 ± 19.4	90.2 ± 25.9	−0.48 ± 0.17	3.95 ± 1.28	22.3 ± 4.48	27.43 ± 0.01	40.81 ± 2.34

slight increase in the surface roughness of the treated surface might be due to the surface reaction of the bioactive glass during the soaking in the $AgNO_3$ solution, the dissolution of the silica structure, and the beginning of the formation of the silica gel, as typical for bioactive glasses [54]. The S_a and S_q values show significant standard deviations. Those can be introduced by the manual gritting process and the quite coarse final gritting paper (#1000), resulting in a certain variability on such small roughness values. Since the reaction of the glass surface, during the ion-exchange process, increases the surface roughness of the samples, it can increase also the standard deviations as well. S_{sk} and S_{ku} parameters provide a deeper insight into the surface structure. A negative S_{sk} indicates that there is a predominance of valleys with respect to peaks on the surface. On the other hand, a S_{ku} value greater than 3 corresponds to sharp and narrow features. Those values originate from the groves left on the surfaces by the SiC particles of the gritting papers. Similar conclusions can be drawn by looking at the amplitude density function (ADF) and the Abbot-Firestone curve, which represent the cumulative ADF, reported in Fig. 3c and d. In both cases, the ADF has a Gaussian-like shape with slightly longer tails below the average line, which corresponds to the peak of the ADF curve. This indicates a higher number of valleys compared to the peaks. The Abbot-Firestone curve shape is in good agreement with the previous considerations. At last, also the ratio between S_q and S_a is close to 1.25, typical for a gaussian topographical profile [55]. In conclusion, the ionic exchange treatment does not seem to affect much the surface morphology of the bioactive glass disks, therefore any difference in the interactions with proteins shall not be ascribed to the micro-topography.

Proteins can interact with biomaterials with different chemical mechanisms. Proteins are usually not chemically homogeneous, they have negatively and positively charged functional groups as well as hydrophobic and hydrophilic domains [35,56]: these moieties differently interact with a surface according to its features [19]. Zeta potential titration curves of the BGs are of interest to investigate the eventual role of the electrostatic protein-surface interaction in adsorption [57,58]. The presence of Ag has a limited effect on the surface ζ potential of the SBA2 glass (Fig. 3e). In the basic range, the two titration curves perfectly overlap, showing the same surface potential, up to about pH 8.5. Above such a value, it is possible that the surfaces start to react, thus showing different behavior. At pH values below 5, the ζ potential of the two surfaces is a bit different. Both surfaces do not reach the isoelectric point in the measured range, indicating the presence of –OH groups with a strong acidic characteristic [59]. These functional groups are deprotonated at low pH values with two different consequences on the titration curve: a shift of the isoelectric point towards pH values lower than 4 and the presence of a plateau with onset at the pH value corresponding to complete deprotonation. The –OH groups on AgSBA2 have a stronger acidic behavior, as indicated by the lower isoelectric point (obtainable from interpolation of the curves with the abscissa) and the onset of the acidic plateau, which starts at a pH lower than the one of SBA2 [60,61]. The different nature of the –OH groups may be related to the contact of the surface with water during the ionic exchange treatment. Furthermore, both glasses are reactive at acidic pH, below 3.5, as evidenced by the increased standard deviations, which indicate that modifications on the surface during the zeta potential measurement occurred on the surface [62].

The measured values for the water contact angle, the dispersive and the polar components of the surface energy are reported in Table 2. Both the glasses show high wettability and hydrophilicity. The presence of –OH groups on both the glass surfaces, as deduced from the zeta potential titration curves, agrees with the measured high wettability. Despite the doping with Ag on the surface of the glass, the contact angle and the surface energy components are not significantly changed. It has been reported that Ag doping via ionic exchange in a high-temperature salt bath can increase surface hydrophobicity [63], but the Ag concentration in AgSBA2 samples may be too low to exert this effect. One of the commonly reported rules of thumb in protein adsorption is that hydrophobic materials form stronger bonds with proteins and that they can bind more proteins with respect to the hydrophilic ones, due to easier displacement of adsorbed water at the interface and entropic gain [64].

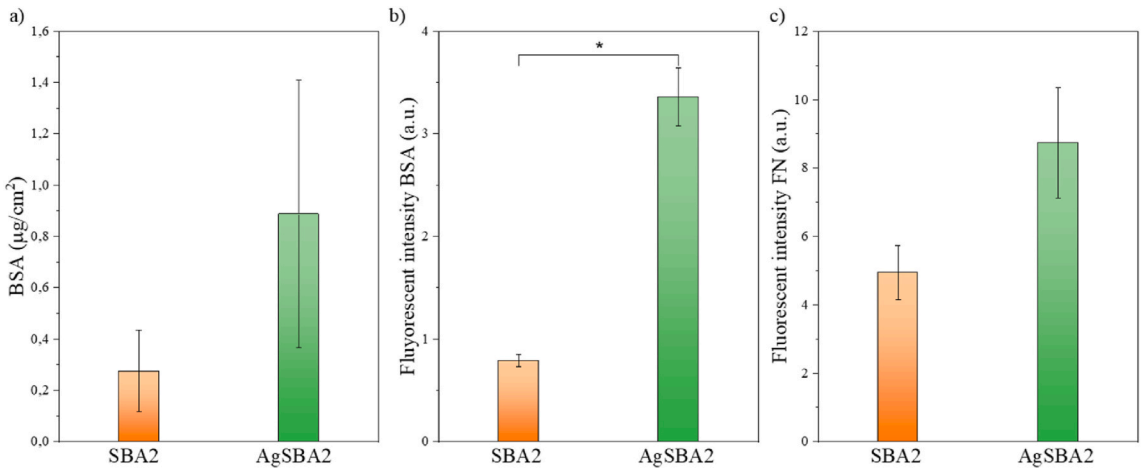

Fig. 4. a) BSA quantification on SBA2 and Ag-SBA2 by BCA assay; fluorescent quantification of adsorbed b) BSA and c) FN. *, $p < 0.05$.

Conversely, it has been demonstrated on other biomaterials, such as polymers or titanium, that higher surface energies can increase the number of proteins adsorbed [65,66]. To the best of the authors' knowledge, no studies about the effect of the surface energy of bioactive glasses on the adsorption of proteins have been reported in the literature and it is of interest for future investigations.

3.2. Quantification of the adsorbed proteins to SBA2 and AgSBA2

The adsorption of BSA and FN, which are very relevant for the osteoimmunomodulation response of the body to a biomedical implant [18], was measured quantitatively in this work by bicinchoninic acid assay (BCA) and fluorescence measurements of labeled proteins and in a semi-quantitative way by XPS.

AgSBA2 adsorbs more BSA with respect to the SBA2 undoped sample (Fig. 4a). The difference between the samples is not statistically significant due to the high standard deviations, mainly detected on AgSBA2. The high standard deviations in the BCA may derive from different factors. At first, due to the quite low overall adsorption, there is possibly an intrinsic variation of the adsorption process, which might not be consistent and well reproducible. As a second and more probable thing, the reaction of the surface and the penetration of BSA inside the silica-gel layer may hinder the effectiveness of SDS to remove the adsorbed proteins from the glass surface. It has been already observed that SDS is unable to completely remove adsorbed proteins from non-reactive surfaces [67]. The protein removal might be even lower on the reactive ones, such as bioactive glasses, leading to underestimating the adsorbed amount.

BSA and FN proteins conjugated with fluorescent markers were used to overcome those limitations. In this case, it was possible to directly quantify the fluorescent signal on the sample's surface, without the need for protein detachment. Furthermore, thanks to the transparency of the glass surface, also the proteins inside the reaction layer can be detected. The results are shown in Fig. 4b and c. The Ag-doped samples showed a greater adsorption capability for both BSA (Fig. 4b) and FN (Fig. 4c), with a fold increase of 4.2 and 1.8 respectively, revealing that the presence of Ag in the bioactive glass surface increases the affinity for proteins as expected from previous studies [31,32]; a minor role of the acidic –OH groups can also be presumed [68,69]. The difference between the two surfaces regarding BSA adsorption is significant ($p < 0,05$), and the standard deviations are lower compared to the ones obtained by the BCA assay. This confirms to some extent that the protein detachment, necessary for performing BCA, may randomly alter the results. Therefore, the use of BCA protein assay for the quantification of adsorbed proteins shall be carefully pondered and the results must be accounted for with proper caution. The underestimation of the adsorption differences between the different specimens may also be related to a different adhesion strength of proteins on the doped/undoped glasses. The strongest bound proteins, as on AgSBA2, may be removed with lower effectiveness by the surfactant with respect to the most loosely adsorbed proteins, as on SBA2, and the amount of proteins detected by BCA is lower as consequence. On the other hand, the adsorption of FN is also higher on the AgSBA2 samples, despite not being statistically significant, indicating that doping with Ag enhances the adsorption of different kinds of proteins in a different way.

Table 3
Carbon and nitrogen atomic concentration on SBA2 and AgSBA2 samples after BSA or FN adsorption.

	C (atomic %)		N (atomic %)	
	BSA	**FN**	**BSA**	**FN**
SBA2	34.10	42.57	2.79	1.55
AgSBA2	37.53	51.26	9.01	0.79

Nitrogen is a typical element of proteins, contained both in the peptidic backbone and lateral groups of some amino acid residues. Since it is not contained in adventitious carbonaceous contaminations, N is usually considered a marker for protein adsorption [70]. The C and N atomic content detected by XPS on SBA2 and AgSBA2 samples after adsorption of BSA and FN are reported in Table 3 and it can be used for a semi-quantitative measurement.

Concerning BGs without proteins (Table S1), the C signal remains almost the same in the case of adsorption on SBA2, while it increases considering BSA and FN on Ag-SBA2. On the other hand, the N signal significantly increased after BSA adsorption on both surfaces and, after FN adsorption, on SBA2. In the case of AgSBA2, the difference in N% before and after FN adsorption is not significant. These facts, combined with the decrease of Si (Table S1), confirm the adsorption of BSA and FN. The N surface percentage corresponding to the complete surface coverage by a BSA layer has been postulated by Foster et al. to be 9% [71], which is well above the values obtained in this work, apart from BSA on AgSBA2. Still, the obtained data need a careful discussion to be properly understood. Bioactive glasses react when in contact with aqueous solutions at physiological pH 7.4, by rapidly forming a hydrated silica-gel layer on the surface and adsorbing PO_4^{3-} ions from the PBS solution, which has a pH of 7.4 as well [72]. The concomitance between those reactions and the adsorption may cause the embedding of the proteins within the gel layer. The capability of XPS to detect elements from a certain depth inside the sample surface relies on the inelastic mean free path (IMPF) of the element electrons: if the depth of the element is higher than the IMPF, the element is not detected. The IMPF,

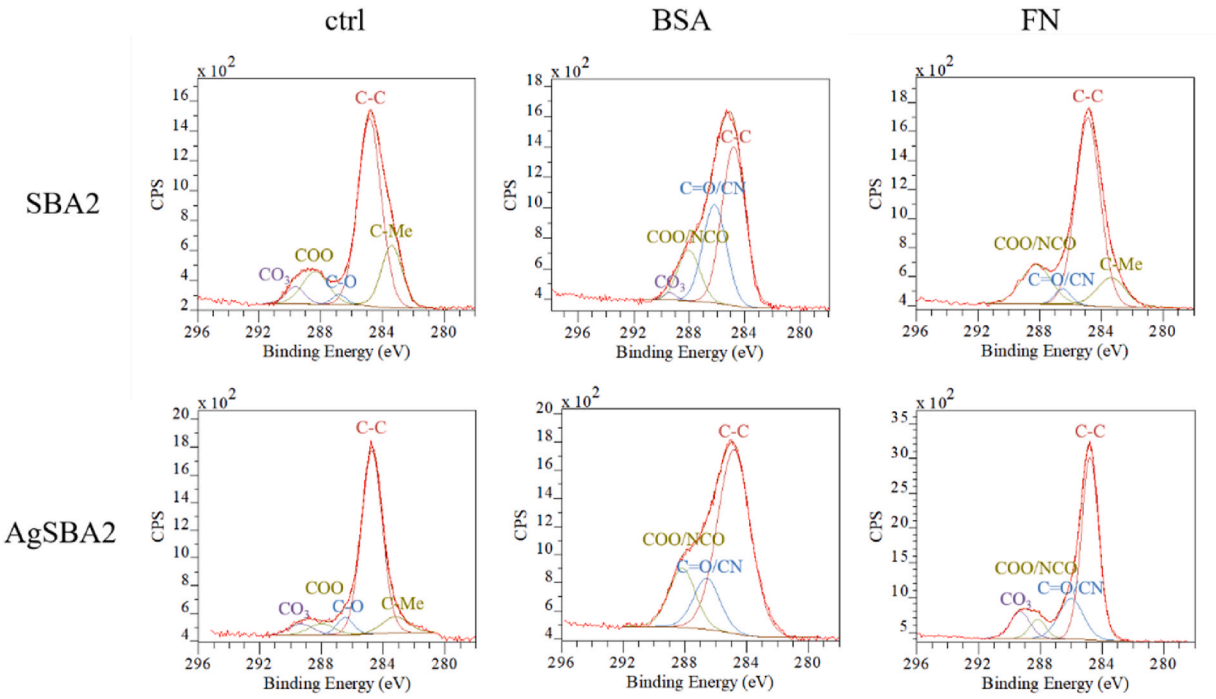

Fig. 5. Deconvolution of high-resolution XPS spectra in the C1s region without (crtl) and with BSA and FN adsorbed on SBA2 and AgSBA2.

among other factors, is determined by the electron kinetic energy and by the composition of the solid the particle is crossing through [73]. In this work, photo-electrons can be emitted from protein molecules within the reacted surface layer. Therefore, they need to travel across a mixed layer of silica gel and organic molecules in order to escape the samples. With respect to the IMPF of electrons, this layer may have an intermediate behavior between pure silicon dioxide, which is the harshest case scenario with the shortest IMPF, and pure proteins, the most favorable scenario with the longest IMPF. N1s core electrons have kinetic energies of about 1088 eV, which correspond to an IMPF shorter than 3 nm in the case of escape through pure silicon dioxide [74]. Similar results can be obtained considering the best scenario, of the electrons travelling through pure proteins [75,76]. In both cases, the IMPF of an N1s core electron can be too short for the electron to escape the silica gel. Therefore, XPS might not provide quantitative information about proteins adsorbed on bioactive glass surfaces, since it is not capable to detect proteins that are embedded within the silica-gel layer. Nevertheless, this fact highlights possible different behaviour of proteins with respect to the hydrated layer: in fact, BSA seems to penetrate less inside the layer, being better detected by XPS, in particular on AgSBA2, while FN may be more incorporated in the reaction layer than be adsorbed on the outermost surface. Another hypothesis is that the amount of BSA on AgSBA2 is high enough to also cover the outermost surface, besides being trapped inside the glass surface layer. The deconvolution of the C1s peaks before and after protein adsorption is reported in Fig. 5. On pristine BGs, environmental carbonaceous contaminations were detected, with peaks at 284.8, 286–287, and 288.2 eV, arising from the -C-C-, –C═O, and carboxyl groups [77]. Other bands were observed, around 283.5 eV and 289.4 eV, which can be attributed to the C-metal bonds and carbonates respectively [78,79]. Those contaminations may arise from residues of the polishing papers and the formation of carbonates during the glass processing. The new contributions which arose after adsorption confirmed the presence of BSA and FN on the surfaces. In fact, the typical peaks of proteins were detected on the glass surfaces, attributed to the C–N signal, between 286 and 287 eV, and the overlapping peaks of N═C–O and COO^- bonds, around 288.1 eV, plus the C–C peak centered at 284.8 eV [47,77,80]. Due to the complexity and reactivity of the system, some other signals are related to contaminations such as carbonates, around 289 eV [79], and carbon-metal bonds, at about 283.3 eV [78], as on the unsoaked surfaces.

The increase of adsorbed proteins on a glass surface doped with Ag agrees with the literature concerning Ag_2O used as a network modifying oxide in different glass systems, silica-based [32] or phosphate-based [31]. The presence of silver, both in the Ag^+ and Ag^0 forms, increases the adsorption of proteins, such as hemoglobin [32] or BSA [31], on glasses according to the silver content. The amount of Ag on the surface of AgSBA2 is similar to the one obtained by using up to 8 mol% of Ag_2O as a modifier in the glass composition [32], which was enough to interact with proteins. Considering the results obtained in the literature and the ones exposed in this work, it can be observed that the effect of Ag on protein adsorption does not depend on how it was introduced inside the BG, if as modifier oxide or by ionic exchange, but more on its chemical state and amount on the surface of the material. The interaction between Ag and the thiol groups of proteins was found to be strong [40] and it is reported to be effective regardless of the number of cysteine residues, the only amino acid bearing a thiol group, in the proteins: hemoglobin has 0.01% of Cys residues [34], BSA 5.8 [81] and FN 2.7 [82]. Moreover, BSA and FN have both a negative net charge at physiological pH (see section 3.5) and AgSBA2 can increase the electrostatic interaction with respect to untreated SBA2 because of the positively charged Ag^+ ions. Increases in protein adsorption due to favorable binding sites was also observed on hydroxyapatite/carbohydroxyapatite precipitated on a bioactive glass exposing different ratios of Ca^{2+}/PO_4^{3-} and $-OH^-$ sites, which change the surface charge: higher adsorption of BSA was observed for the more positively charged nanostructure [41]. The quantification of the adsorbed plasma proteins is of biological relevance because they are well known to modulate cellular reactions [30]. Previous work from the authors [83] showed that SBA2 and AgSBA2 have similar cytocompatibility regarding human osteoblasts progenitors (hFOB). Furthermore, cell viability is enhanced on AgSBA2 with respect to SBA2 when an infection of a healing implant is simulated, by adding an aliquot of an infected medium, containing *Staphylococcus aureus*, to a cell culture where hFOB were previously seeded on the glass samples [83]. The increased affinity towards adhesive proteins, such as FN [84], of the Ag-doped surface, may concur to

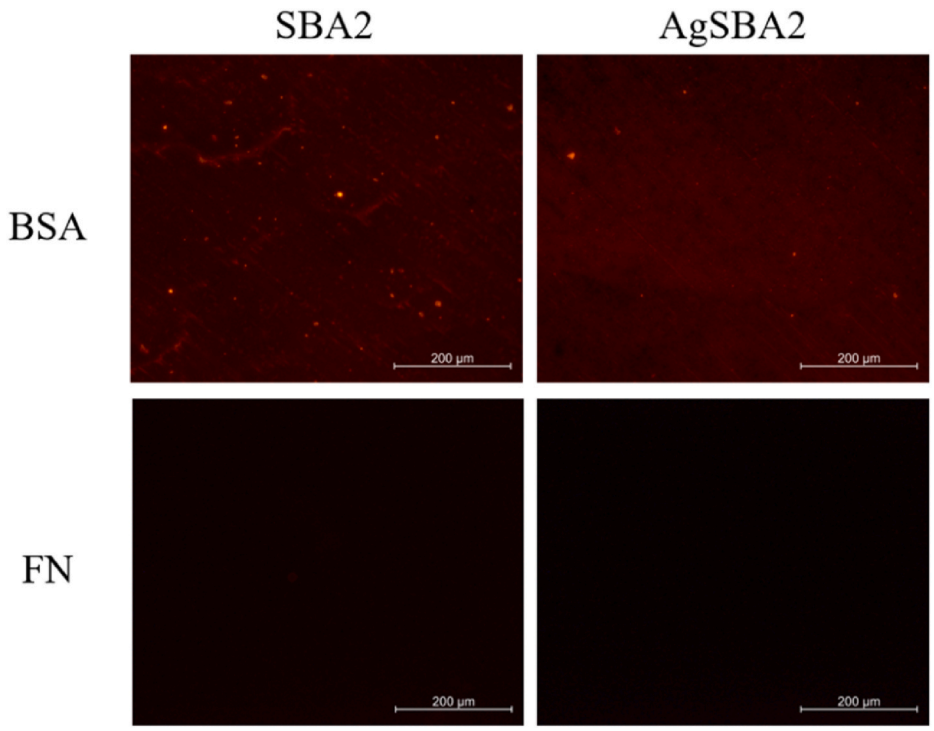

Fig. 6. Fluorescent imaging of protein adsorbed on SBA2 and AgSBA2 surfaces (magnification 200×).

increase the cellular response, along with the antibacterial effect. Furthermore, the adsorption of anti-inflammatory proteins, as in the case of BSA [85], can inhibit the acute phase of the inflammatory response of the body, leading to an improved osteoimmunomodulation ability of this biomaterial [86].

3.3. Protein layers on the glass surfaces

One of the crucial aspects of the adsorption of proteins is the degree of coverage of the surface. The distribution of adsorbed BSA and FN was investigated at two different scales, thanks to fluorescent proteins and a novel approach by KPFM, developed by the authors in previous work [87].

Fluorescent images are reported in Fig. 6. It is possible to see that BSA forms a continuous and mainly homogeneous layer on both surfaces. On SBA2, preferential adsorption along the polishing grooves is observed, indicating that microroughness may have an enhancing effect on protein adsorption to some extent, acting as a sort of protein reservoir. On the other hand, the same effect is not noticed in the AgSBA2 sample: the effect of the topography is less significant in this case due to the increased adsorption capability of the Ag-doped surface. While the BSA signal was well acquired and imaged, the detected signal from fluorescent FN was insufficient to formulate any conclusion (Fig. 6). Contrary with respect to the Chemidoc system, the maximum exposure time exploitable in the fluorescent microscope was not sufficient to acquire images from the adsorbed FN on the glass samples. The absence of features in the fluorescent images suggests that the adsorption is homogeneous, without the formation of aggregates and the presence of FN in a buried layer, and surface reactivity could explain the low intensity of the signal. However, it would be hazardous to hypothesize about the extent of the surface coverage using this technique.

To characterize the extension and the morphology of the protein layers formed after adsorption, Kelvin probe force microscopy was applied. This atomic force microscopy technique allows to image the

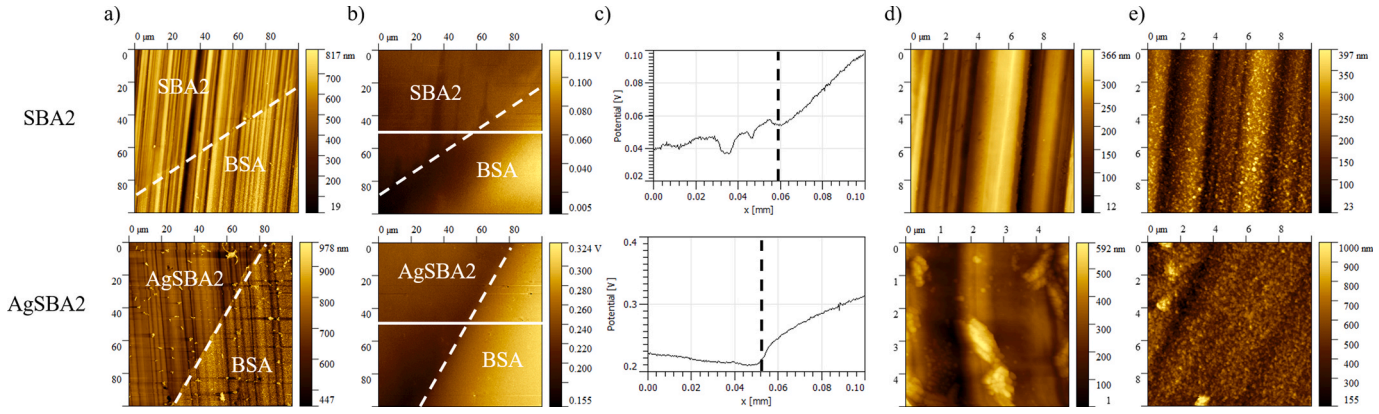

Fig. 7. Kelvin probe force microscopy images of SBA2 and AgSBA2 after BSA adsorption on a portion of the surface: a)100 × 100 μm scan topography; b) 100 × 100 μm scan surface potential; c) potential profile along the white line in the potential image (the black dotted vertical line represents the boundary of the region with BSA); d) 5 × 5 μm scan of pristine surface; e) 5 × 5 μm scan of BGs with BSA. BSA is adsorbed at the right of the large scan, as indicated in the pictures.

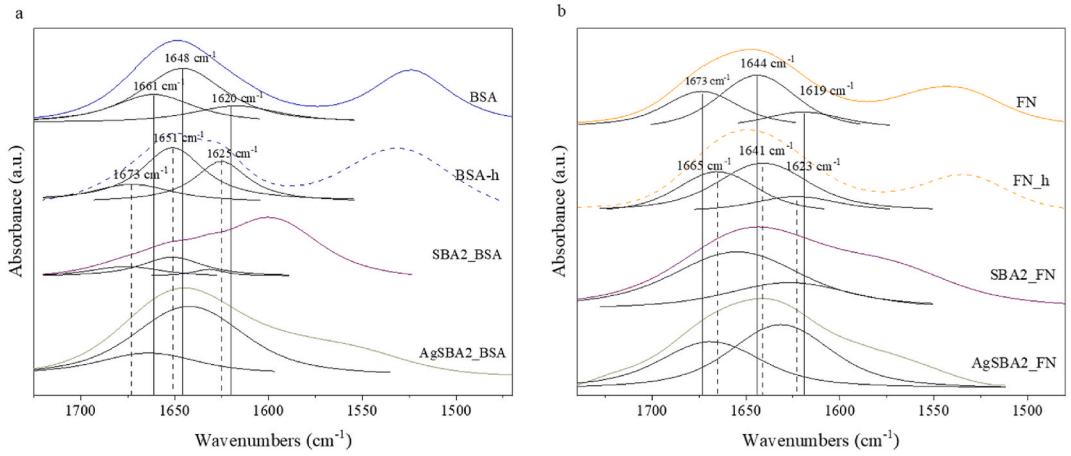

Fig. 8. Deconvolution of the Amide I band FTIR spectra for BSA (a) and FN (b), in the native (BSA and FN) and denatured state (BSA_h and FN_h) and after adsorption on SBA2 and AgSBA2. The position of the components of the native or denatured proteins is marked with solid or dashed lines respectively.

surface potential of a sample and it was recently applied for visualizing protein adsorption on flat model substrates [88,89] or on rough titanium substrates, which underwent surface chemical modification for osseointegration purposes [87].

Fig. 7 reports the topographical and surface potential images for BSA adsorbed on the two glasses. The samples used for this analysis were prepared with a limited area exposed to protein adsorption to use the unadsorbed area as an internal control (see the Materials and Methods section). The results obtained in terms of morphology and potential distribution are similar in all the cases. The areas of the bioactive glasses that have been exposed to the protein solution are distinguishable by looking both at the topography and surface potential images. During the adsorption of proteins from the PBS solution, the glasses begin to dissolve and form the silica-gel layer, with a concomitant increase in the surface roughness that is visible in the topographical images at high magnification (Fig. 7d vs Fig. 7e). Interestingly, the reaction of the glass leads also to an increase in the height of the surface, since a step of 70–100 nm was found between the soaked and unsoaked areas, which can be correlated to an increased volume of the hydrated silica-gel with respect to the unreacted glass surface. The thickness of the reaction layer here detected can justify the low detection of nitrogen by XPS, as discussed before, since it is much larger than the IMPF of the N1s electrons [74,75]. According to the literature, this reaction layer is formed through various steps: at first, $Si(OH)_4$ groups solubilize from the surface after the dissolution of the glass network; in second place, the solubilized silica groups polymerize and reprecipitate on the surface [54]. The reactions occurring during protein adsorption also affect the surface potential images (Fig. 7c). The combined protein-silica layer has a higher potential than the intact surface and no formation of aggregates of proteins is evidenced by KPFM. Very similar results were obtained in the case of KPFM performed after FN adsorption and are not shown here for sake of concision.

The fluorescence and AFM/KPFM images correlate with each other and support the observation and hypothesis discussed in the previous section. Since proteins are adsorbed contemporary to the formation of the silica-gel layer, it is plausible that they are at least partially embedded within the reaction layer, forming a continuous silica-gel/protein composite film. This is of biological relevance because, whether or not the protein layer is complete, determines if the cells interact with the adsorbed proteins or directly with the biomaterial [90]. As an example of the biological effect of a differential protein adsorption, a titanium surface modified with a pattern where protein adsorption was localized in some areas showed a subsequent patterned proliferation and differentiation of MC3T3-E1 pre-osteoblast cells, enhancing the formation of bone nodules where proteins adsorption was higher [91].

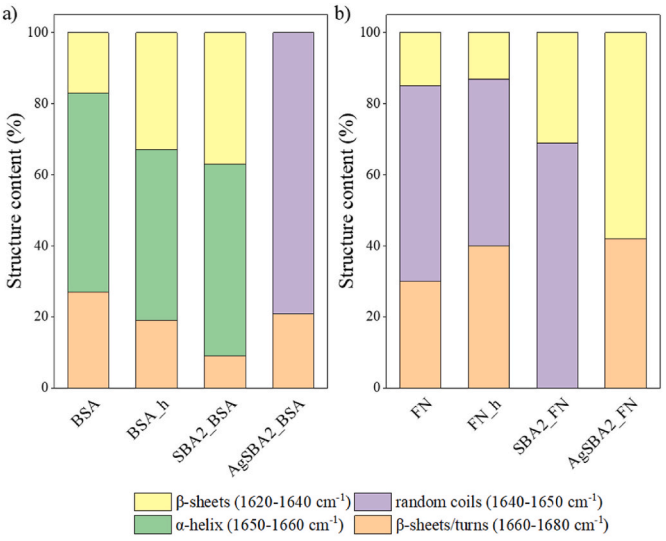

Fig. 9. Secondary structure of BSA and FN adsorbed on BSA2 and AgSBA2. The structure of the proteins before and after thermal denaturation is also reported.

3.4. Protein secondary structure

The effect of Ag doping of the glass on the conformation of the adsorbed proteins, which may translate into a different cell response to the biomaterial itself, has been investigated by ATR-FTIR. After adsorption, the main signals of proteins were detected on SBA2 and AgSBA2, while soaking the samples in a simple PBS solution, without proteins, does not generate strong interfering bands (Fig. S2). Amide I and Amide II bands are respectively around 1650 cm^{-1} and 1450 cm^{-1} and arise from the vibration of –C═O or –CN and –NH bonds [92]. As discussed in the supporting information, the Amide II band was hardly detected due to the low amount of proteins adsorbed on the surface and the presence of interfering bands from the reaction layer on the bioactive glasses. The Amide I band is the most sensitive to the protein secondary structure [31,92,93] and it has been exploited to investigate the secondary structure of the proteins after adsorption on the glass surface without or with Ag doping, the results are presented in Fig. 8. A certain frequency range of the FTIR spectra can be assigned to each secondary structure of proteins According to the literature, β-sheet structures were assigned to bands in the range from 1620 to 1640 cm^{-1}, the 1640-1650

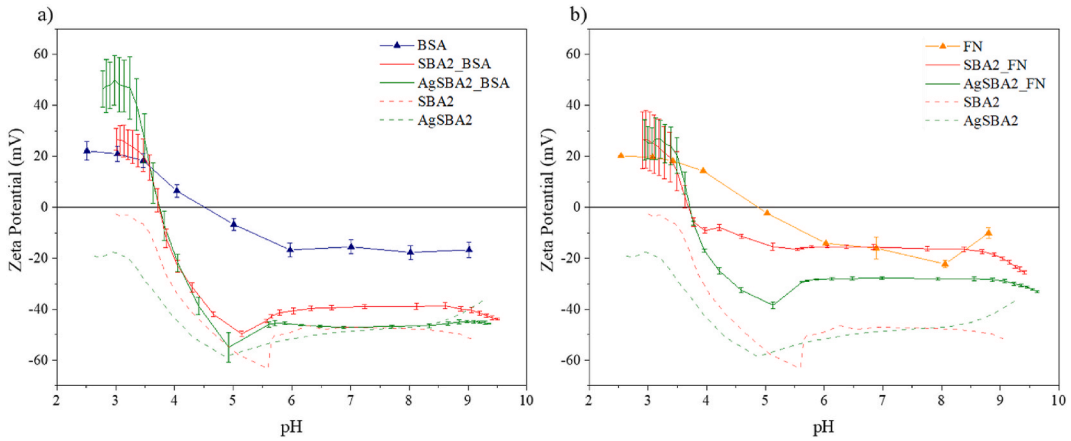

Fig. 10. Zeta potential vs pH curves of glass surfaces after adsorption of BSA (a) and FN (b). The zeta potential titration curves for BSA and FN in solution and BG surfaces before adsorption are also reported.

cm^{-1} bands correspond to random coils, the signal between 1650 and 1660 cm^{-1} is due to α-helices and the highest wavenumber component, between 1660 and 1680 cm^{-1}, is related to a combination of β-sheet and β-turn structures [31,93–96]. The different contributions to the Amide I band obtained after deconvolution are shown in Fig. 9.

When BSA is adsorbed onto the undoped glass surface (Figs. 8a and 9a and Table S2), the overall quantities of α-helices and β-structures are similar to the case of native BSA, even though the presence of the overlapping OH band (around 1600 cm^{-1}) [97], affects the accurate definition of the Amide I band position and components, in this case. A possible decrease in β-turns can be supposed. On the other hand, the BSA structure drastically changes after adsorption on the AgSAB2 sample, seeming to have completely lost the α-helical structures with the concomitant formation of random coils, with their signal centered at about 1640 cm^{-1}, β-sheets and β-turns (at 1663 cm^{-1}). The same structures appear after the thermal denaturation of BSA, with the formation of β-sheets in agreement with some results reported in the literature [98].

In the case of FN (Figs. 8b and 9b and Table S2), some changes in the secondary structure of the protein were observed after adsorption on both surfaces but showed different behaviour. On the SBA2 surface, only random coils (signal around 1655 cm^{-1}), and β-sheets structures (around 1626 cm^{-1}) were observed. On the other hand, FN secondary structure is composed of β-sheets and β-turns, and no random coils were observed after interaction with AgSBA2. No component was assigned to α-helical structures in all cases since they are not in the native structure of FN [99].

Despite the low amount of proteins adsorbed on the glass samples, and the presence of some signals deriving from the reactions of the material surface during immersion in aqueous solutions, which partially interfere with the exact quantitative determination of the secondary structure of the adsorbed proteins, interesting information about the denaturation of BSA and FN after interaction with the bioactive glass surfaces were obtained. The spectral deconvolution of adsorbed BSA shows that it mainly retains its native conformation when interacting with SBA2, while it gets heavily denatured after adsorption on the Ag-containing surface. The ability of Ag to bind thiol groups of amino acids is well acknowledged and it's reported to have an active role in the antibacterial effect of Ag, by compromising the biological functions of bacteria membrane proteins [100]. The great loss of the ordered structure of BSA after adsorption on AgSBA2 can be due to this kind of strong interaction. Ag is capable also to break the disulphide bridges between cysteine residues in the BSA chain, mainly when it is in the form of metallic Ag^0 [31], after interacting with the free –SH groups of the proteins. Furthermore, surface charge and protein-material electrostatic interaction have been found to play a role in the structural stability of adsorbed proteins [41] and it was observed that surfaces with a positive charge reduce the amount of α-helical structure in the adsorbed proteins [101]. This factor can also concur with the denaturation of BSA through the positive Ag^+ ions. BSA denaturation was correlated to a better cellular attachment [41], and the loss of native conformation detected here can explain the better osteoblast response to AgSBA2 previously observed [83]. The secondary structure of FN was changed after adsorption on both surfaces. The presence of Ag in the glass seems to promote the formation of β-sheets, as in the case of BSA, by ordering random coil portions of the polypeptide chain. On the other hand, SBA2 can promote the disruption of the ordinate structure with the increase of random coils. In this case, the differences between the behavior of FN on SBA2 and AgSBA2 can be less ascribed to the interaction between the thiol groups and Ag due to the lower amount of cysteine. The different denaturation can be the result of stronger electrostatic interactions between the Ag^+ ions and FN $–COO^-$ groups. The biological activity of proteins is strictly related to their tertiary structure and to the active amino acid sequences that can be recognized by cell membrane receptors. Ag-induced denaturation of proteins can be beneficial for the *in vivo* response to BGs, even though it has been claimed that the optimal Ag concentration is the one that enhances protein adsorption limiting the denaturation [31]. For example, it is well established that FN needs to partially expand to expose the RGD sequence (a tripeptide arginine-glycine-aspartate) in order to accomplish its role as an adhesive protein [102–104]. In fact, the RGD sequence can bind to α5β1 integrins on the cell membrane, with a synergic action of a further aminoacidic sequence (proline-histidine-serine-arginine-asparagine), promoting cell adhesion and spreading [99]. The exposure of the RGD sites and, consequently, the enhanced cell interaction is dependent on the conformation and orientation of FN dimers upon adsorption, which is dictated by the surface properties [105]. The presence of Ag in the BG surface seems to provide a certain selectivity in the interactions with proteins. The higher the number of thiol groups in the proteins, the highest the amount of adsorbed protein (Fig. 4) and the greater their denaturation (Fig. 8) when compared to proteins onto the undoped glass. The possibility to tune the interactions with proteins is very intriguing for the engineering of novel biomaterial surfaces, opening new horizons in tailoring the tissue response to implants.

3.5. Zeta potential of the adsorbed proteins

Zeta potential measurement is very sensitive to the surface chemistry and, despite being usually employed to characterize surface properties of colloids [106], it is also reported to be useful for the investigation of protein adsorption on different surfaces, such as titanium oxide [57], treated titanium alloys [44], and SiO_2 [107].

Table 4
Nitrogen concentration on SBA2 and AgSBA2 samples with adsorbed BSA or FN after zeta potential measure in the acidic range.

	N (atomic %)	
	BSA	FN
SBA2_z	1.30	4.18
AgSBA2_z	7.27	6.22

The zeta potential titration curves for SBA2 and AgSBA2 after adsorption are reported in Fig. 10. In both cases, the curves of the adsorbed proteins are quite different from the ones of proteins suspended in aqueous solutions. After BSA adsorption (Fig. 10a), the curves of SBA2_BSA and AgSBA2-BSA overlap almost perfectly. With respect to the uncovered surface, the main change is that the IEP is detected at a pH value of 3.7 and that the potential of the SBA2 at basic pH increased. The adsorption of FN provoked similar a change (Fig. 10b) concerning the shift of the IEPs to a pH equal to 3.7. However, the curves of SBA2_FN and AgSBA2_FN are quite different at pH higher than the IEP, with AgSBA2_FN having a more negative surface. In all cases, there is an increase in the standard deviations at pH around the IEP, which may be due to a reaction of the surface during the measures [62].

The zeta potential of a surface depends on its functional groups and eventual ions exposed. In the case of proteins and glass surfaces, those are mainly the carboxyl -COO^- and protonated amino groups –NH_3^+ of the proteins or hydroxyl groups of the silica surface, as commented in section 3.1. The amino groups of proteins are in the protonated form over all the considered pH range, since they have a $pK_a > 9$, while the carboxyl groups ($pK_a \approx 4$) begin to be protonated at pH lower than 5 and they are all in the –COOH form at pH around 3 [108], corresponding to the acidic plateau detected in the titration curves of the proteins in solution. Due to the growth of the silica-gel layer in concomitance with the adsorption process and the likely exposition on the surface of the functional groups both of the glass and proteins, it is not possible to distinguish their contributions to the overall titration curves. Nevertheless, looking at the similarities between the curves it is possible to hypnotize that the surface layer combining adsorbed proteins and the silica-gel has comparable chemistry in the case of BSA. The higher potential for SBA2_FN with respect to AgSBA2_FN might be due to some differences in the interaction with FN and the glass surfaces and the resulting protein orientation or folding, as observed by the authors in a previous work regarding other biomaterials [69], or to the different presence of ions on the glass surface (Table S1).

In order to better understand how the glass surface reacts during the potential measurements, XPS analyses were performed on the samples subjected to the acidic range of the titration curve, in particular, to observe whether or not proteins are removed from the surfaces during the titration. Very unexpected results were obtained for the nitrogen concentrations, reported in Table 4. While the signal of the BSA N1s decreases after the zeta potential measurement, as expected since the electrolyte flow can mechanically remove proteins from the sample surfaces, the N signal from FN is highly increased. In the meantime, Si is more present on all the surfaces and other elements, such as Ca and P, are hardly detected (Table S1).

The results obtained on the BSA covered samples suggest that a certain amount of protein is removed from the glass surfaces, due to the electrolyte flow and pH, which is a predictable outcome. On the other hand, the increase of nitrogen concentration on surfaces adsorbed with FN was completely unanticipated since the electrolyte solution for the zeta potential does not contain any protein. A possible explanation is that the combination of the shear stress applied to the surface by the electrolyte and the acidic environment can remove the outermost layer of the samples, which might be mainly composed of silica-gel, environmental contaminations, and some precipitates, such as phosphates and Ca^{2+} ions, exposing in a larger amount the proteins originally embedded within the surface reaction layer. These results are very interesting, since they confirm and highlight the very complex interplay between the reactive surface of bioactive glass and proteins contained in biological fluids, and they certify that proteins penetrate inside the hydrated silica-gel layer during the reaction occurring while soaking in the protein solution (Fig. 11), as suggested by Effah Kaufmann et al. [37].

4. Conclusions

In the present paper, the effect of Ag doping on the adsorption of serum proteins, which are relevant for the *in vivo* osseointegration of biomaterials, has been investigated on a silica-based bioactive glass surface doped through an ionic-exchange treatment. The effect of Ag on the behavior of two different proteins, BSA and FN respectively, has been compared here for the first time. It was observed that the presence of Ag does not affect the overall surface properties of the bioactive glass, such as roughness or surface energy, but slightly changes the ζ potential, introducing more acidic –OH groups. However, the Ag-containing BG shows significantly higher adsorption of BSA and FN with respect to the unmodified glass system. Furthermore, the secondary structure of the adsorbed proteins is more changed when interacting with the AgSBA2 samples. These results confirm the role of Ag in protein adsorption and provide more insight into the concomitant occurrence of protein adsorption and the formation of a surface reaction layer on bioactive glasses. In fact, proteins can be embedded within the silica-gel layer that forms on bioactive glasses in contact with aqueous solutions. A different penetration capability was also highlighted: BSA remains more on the outermost layer of the glass surface, while FN penetrates more inside the reaction layer. The actual interface between the cells and the bioactive glass may be composed of the silica-gel reaction layer containing embedded proteins. The improved protein affinity of bioactive glasses treated with the ionic exchange may be beneficial for the cellular and anti-infection response and can lead to advances in the design of novel compositions of bioactive glasses. The selectivity of AgBSA2 towards cysteine-containing proteins is also an outcome of great interest.

Authors contributions

Conceptualization: Silvia Spriano, Jacopo Barberi; Funding acquisition: Silvia Spriano, Andrea Mario Rossi, Seiji Yamaguchi; Investigation: Jacopo Barberi, Luisa Mandrile, Lucia Napione, Alessandra Vitale; Methodology: Silvia Spriano, Luisa Mandrile, Andrea Mario Giovannozzi, Marta Miola, Lucia Napione; Supervision: Silvia Spriano, Andrea Mario Rossi; Writing-original draft: Jacopo Barberi; Writing-review & editing: All authors.

Declaration of competing interest

The authors declare that they have no known competing financial

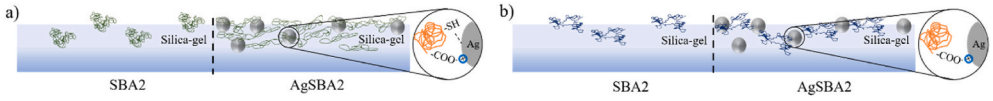

Fig. 11. Representation of the final structure of the combined protein-silica gel layer in case of (a) and FN (b) adsorption on SBA2 and AgSAB2 respectively. In every case, proteins are adsorbed both on the surface and inside the silica-gel layer. The supposed interaction mechanisms with Ag are also represented: BSA interacts with Ag both with thiol groups and electrostatically, with high adsorption enhancement and denaturation; FN has mainly electrostatic interactions, with moderate adsorption enhancement and denaturation.

interests or personal relationships that could have appeared to influence the work reported in this paper.

Acknowledgements

This research was in part performed in the IMPreSA Infrastructure laboratories, funded by Regione Piemonte and INRIM. This research did not receive any specific grant from funding agencies in the public, commercial, or not-for-profit sectors.

Appendix A. Supplementary data

Supplementary data to this article can be found online at https://doi.org/10.1016/j.ceramint.2022.12.251.

References

[1] M.G. Kaufman, J.D. Meaike, S.A. Izaddoost, Orthopedic prosthetic infections: diagnosis and orthopedic salvage, Semin. Plast. Surg. 30 (2016) 66–72, https://doi.org/10.1055/s-0036-1580730.

[2] M. Vallet-Regí, D. Lozano, B. González, I. Izquierdo-Barba, Biomaterials against bone infection, Adv. Healthc. Mater. 9 (2020), https://doi.org/10.1002/adhm.202000310.

[3] M.S. Morehead, C. Scarbrough, Emergence of global antibiotic resistance, Prim. Care Clin. Off. Pract. 45 (2018) 467–484, https://doi.org/10.1016/j.pop.2018.05.006.

[4] D.R. Dodds, Antibiotic resistance: a current epilogue, Biochem. Pharmacol. 134 (2017) 139–146, https://doi.org/10.1016/j.bcp.2016.12.005.

[5] A. Bistolfi, G. Massazza, E. Verné, A. Massè, D. Deledda, S. Ferraris, M. Miola, F. Galetto, M. Crova, Antibiotic-loaded cement in orthopedic surgery: a review, ISRN Orthop 2011 (2011) 1–8, https://doi.org/10.5402/2011/290851.

[6] M. Cazzola, S. Ferraris, V. Allizond, C.M. Bertea, C. Novara, A. Cochis, F. Geobaldo, A. Bistolfi, A.M. Cuffini, L. Rimondini, G. Banche, S. Spriano, Grafting of the peppermint essential oil to a chemically treated Ti6Al4V alloy to counteract the bacterial adhesion, Surf. Coating. Technol. 378 (2019), https://doi.org/10.1016/j.surfcoat.2019.125011.

[7] J. Hasan, R.J. Crawford, E.P. Ivanova, Antibacterial surfaces: the quest for a new generation of biomaterials, Trends Biotechnol. 31 (2013) 295–304, https://doi.org/10.1016/j.tibtech.2013.01.017.

[8] S.V.V.S.N. Narayana, S.V.V.S. Srihari, A review on surface modifications and coatings on implants to prevent biofilm, Regen. Eng. Transl. Med. 6 (2020) 330–346, https://doi.org/10.1007/s40883-019-00116-3.

[9] J.A. Del Olmo, L. Ruiz-Rubio, L. Pérez-Alvarez, V. Sáez-Martínez, J.L. Vilas-Vilela, Antibacterial coatings for improving the performance of biomaterials, Coatings 10 (2020), https://doi.org/10.3390/coatings10020139.

[10] V. Mouriño, J.P. Cattalini, A.R. Boccaccini, Metallic ions as therapeutic agents in tissue engineering scaffolds: an overview of their biological applications and strategies for new developments, J. R. Soc. Interface 9 (2012) 401–419, https://doi.org/10.1098/rsif.2011.0611.

[11] J. Quinn, R. McFadden, C.W. Chan, L. Carson, Titanium for orthopedic applications: an overview of surface modification to improve biocompatibility and prevent bacterial biofilm formation, iScience 23 (2020), https://doi.org/10.1016/j.isci.2020.101745.

[12] H. Lu, Y. Liu, J. Guo, H. Wu, J. Wang, G. Wu, Biomaterials with antibacterial and osteoinductive properties to repair infected bone defects, Int. J. Mol. Sci. 17 (2016), https://doi.org/10.3390/ijms17030334.

[13] S.M. Rabiee, N. Nazparvar, M. Azizian, D. Vashaee, L. Tayebi, Effect of ion substitution on properties of bioactive glasses: a review, Ceram. Int. 41 (2015) 7241–7251, https://doi.org/10.1016/j.ceramint.2015.02.140.

[14] J.S. Fernandes, P. Gentile, R.A. Pires, R.L. Reis, P.V. Hatton, Multifunctional bioactive glass and glass-ceramic biomaterials with antibacterial properties for repair and regeneration of bone tissue, Acta Biomater. 59 (2017) 2–11, https://doi.org/10.1016/j.actbio.2017.06.046.

[15] U. Pantulap, M. Arango-Ospina, A.R. Boccaccini, Bioactive glasses incorporating less-common ions to improve biological and physical properties, J. Mater. Sci. Mater. Med. 33 (2022) 3, https://doi.org/10.1007/s10856-021-06626-3.

[16] A. Moghanian, S. Nasiripour, S.M. Hosseini, S.H. Hosseini, A. Rashvand, A. Ghorbanoghli, A. Pazhouheshgar, F. Sharifian Jazi, The effect of Ag substitution on physico-chemical and biological properties of sol-gel derived 60% SiO2-31%CaO-4%P2O5-5%TiO2 (mol%) quaternary bioactive glass, J. Non-Cryst. Solids 560 (2021), 120732, https://doi.org/10.1016/j.jnoncrysol.2021.120732.

[17] S. Di Nunzio, C. Vitale Brovarone, S. Spriano, D. Milanese, E. Verné, V. Bergo, G. Maina, P. Spinelli, Silver containing bioactive glasses prepared by molten salt ion-exchange, J. Eur. Ceram. Soc. 24 (2004) 2935–2942, https://doi.org/10.1016/j.jeurceramsoc.2003.11.010.

[18] Z. Chen, T. Klein, R.Z. Murray, R. Crawford, J. Chang, C. Wu, Y. Xiao, Osteoimmunomodulation for the development of advanced bone biomaterials, Mater. Today 19 (2016) 304–321, https://doi.org/10.1016/j.mattod.2015.11.004.

[19] M. Rabe, D. Verdes, S. Seeger, Understanding protein adsorption phenomena at solid surfaces, Adv. Colloid Interface Sci. 162 (2011) 87–106, https://doi.org/10.1016/j.cis.2010.12.007.

[20] J.M. Anderson, A. Rodriguez, D.T. Chang, Foreign body reaction to biomaterials, Semin. Immunol. 20 (2008) 86–100, https://doi.org/10.1016/j.smim.2007.11.004.

[21] E. Mariani, G. Lisignoli, R.M. Borzì, L. Pulsatelli, Biomaterials: foreign bodies or tuners for the immune response? Int. J. Mol. Sci. 20 (2019) https://doi.org/10.3390/ijms20030636.

[22] H.P. Felgueiras, J.C. Antunes, M.C.L. Martins, M.A. Barbosa, Fundamentals of Protein and Cell Interactions in Biomaterials, Elsevier Ltd., 2018, https://doi.org/10.1016/B978-0-08-100803-4.00001-2.

[23] J. Chang, X. Zhang, K. Dai, Material characteristics, surface/interface, and biological effects on the osteogenesis of bioactive materials, in: Bioact. Mater. Bone Regen., Elsevier, 2020, pp. 1–103, https://doi.org/10.1016/B978-0-12-813503-7.00001-7.

[24] V. Arroyo, R. García-Martinez, X. Salvatella, Human serum albumin, systemic inflammation, and cirrhosis, J. Hepatol. 61 (2014) 396–407, https://doi.org/10.1016/j.jhep.2014.04.012.

[25] Y. Yang, Y. Xiao, Biomaterials regulating bone hematoma for osteogenesis, Adv. Healthc. Mater. 9 (2020), https://doi.org/10.1002/adhm.202000726.

[26] L. Badihi Hauslich, M.N. Sela, D. Steinberg, G. Rosen, D. Kohavi, The adhesion of oral bacteria to modified titanium surfaces: role of plasma proteins and electrostatic forces, Clin. Oral Implants Res. 24 (2013) 49–56, https://doi.org/10.1111/j.1600-0501.2011.02364.x.

[27] J. Barberi, S. Spriano, Titanium and protein adsorption: an overview of mechanisms and effects of surface features, Materials 14 (2021) 1590, https://doi.org/10.3390/ma14071590.

[28] Y. Hedberg, X. Wang, J. Hedberg, M. Lundin, E. Blomberg, I. Odnevall Wallinder, Surface-protein interactions on different stainless steel grades: effects of protein adsorption, surface changes and metal release, J. Mater. Sci. Mater. Med. 24 (2013) 1015–1033, https://doi.org/10.1007/s10856-013-4859-8.

[29] W.H. Lee, C.Y. Loo, R. Rohanizadeh, A review of chemical surface modification of bioceramics: effects on protein adsorption and cellular response, Colloids Surf. B Biointerfaces 122 (2014) 823–834, https://doi.org/10.1016/j.colsurfb.2014.07.029.

[30] K. Zheng, M. Kapp, A.R. Boccaccini, Protein interactions with bioactive glass surfaces: a review, Appl. Mater. Today 15 (2019) 350–371, https://doi.org/10.1016/j.apmt.2019.02.003.

[31] K. Magyari, C. Gruian, B. Varga, R. Ciceo-Lucacel, T. Radu, H.J. Steinhoff, G. Váró, V. Simon, L. Baia, Addressing the optimal silver content in bioactive glass systems in terms of BSA adsorption, J. Mater. Chem. B. 2 (2014) 5799–5808, https://doi.org/10.1039/c4tb00733f.

[32] A. Vulpoi, C. Gruian, E. Vanea, L. Baia, S. Simon, H.J. Steinhoff, G. Göller, V. Simon, Bioactivity and protein attachment onto bioactive glasses containing silver nanoparticles, J. Biomed. Mater. Res., Part A 100 A (2012) 1179–1186, https://doi.org/10.1002/jbm.a.34060.

[33] C. Gruian, A. Vulpoi, E. Vanea, B. Oprea, H.J. Steinhoff, S. Simon, The attachment affinity of hemoglobin toward silver-containing bioactive glass functionalized with glutaraldehyde, J. Phys. Chem. B 117 (2013) 16558–16564, https://doi.org/10.1021/jp408830t.

[34] C. Gruian, A. Vulpoi, H.J. Steinhoff, S. Simon, Structural changes of methemoglobin after adsorption on bioactive glass, as a function of surface functionalization and salt concentration, J. Mol. Struct. 1015 (2012) 20–26, https://doi.org/10.1016/j.molstruc.2012.01.045.

[35] A. Bujacz, Structures of bovine, equine and leporine serum albumin, Acta Crystallogr. Sect. D Biol. Crystallogr. 68 (2012) 1278–1289, https://doi.org/10.1107/S0907444912027047.

[36] The UniProt Consortium, UniProt: the universal protein knowledgebase in 2021, Nucleic Acids Res. 49 (2021) D480–D489, https://doi.org/10.1093/nar/gkaa1100.

[37] E.A.B. Effah Kaufmann, P. Ducheyne, S. Radin, D.A. Bonnell, R. Composto, Initial events at the bioactive glass surface in contact with protein-containing solutions, J. Biomed. Mater. Res. 52 (2000) 825–830, https://doi.org/10.1002/1097-4636(20001215)52:4<825::AID-JBM28>3.0.CO;2-M.

[38] H.M.W. Uyen, J.M. Schakenraad, J. Sjollema, J. Noordmans, W.L. Jongebloed, I. Stokroos, H.J. Busscher, Amount and surface structure of albumin adsorbed to solid substrata with different wettabilities in a parallel plate flow cell, J. Biomed. Mater. Res. 24 (1990) 1599–1614, https://doi.org/10.1002/jbm.820241205.

[39] D.M. Togashi, A.G. Ryder, G. Heiss, Quantifying adsorbed protein on surfaces using confocal fluorescence microscopy, Colloids Surf. B Biointerfaces 72 (2009) 219–229, https://doi.org/10.1016/j.colsurfb.2009.04.007.

[40] R. Veres, D.L. Trandafir, K. Magyari, S. Simon, D. Barbos, V. Simon, Gamma irradiation effect on bioactive glasses synthesized with polyethylene-glycol template, Ceram. Int. 42 (2016) 1990–1997, https://doi.org/10.1016/j.ceramint.2015.10.004.

[41] U. Thamma, T.J. Kowal, M.M. Falk, H. Jain, Nanostructure of bioactive glass affects bone cell attachment via protein restructuring upon adsorption, Sci. Rep. 11 (2021) 5763, https://doi.org/10.1038/s41598-021-85050-7.

[42] M. Miola, G. Fucale, G. Maina, E. Verné, Composites bone cements with different viscosities loaded with a bioactive and antibacterial glass, J. Mater. Sci. 52 (2017) 5133–5146, https://doi.org/10.1007/s10853-017-0750-1.

[43] M. Miola, G. Fucale, G. Maina, E. Verné, Antibacterial and bioactive composite bone cements containing surface silver-doped glass particles, Biomed. Mater. 10 (2015), https://doi.org/10.1088/1748-6041/10/5/055014.

[44] S. Ferraris, M. Cazzola, V. Peretti, B. Stella, S. Spriano, Zeta potential measurements on solid surfaces for in Vitro biomaterials testing: surface charge, reactivity upon contact with fluids and protein absorption, Front. Bioeng. Biotechnol. 6 (2018) 1–7, https://doi.org/10.3389/fbioe.2018.00060.
[45] A. Rudawska, E. Jacniacka, Analysis for determining surface free energy uncertainty by the Owen–Wendt method, Int. J. Adhesion Adhes. 29 (2009) 451–457, https://doi.org/10.1016/j.ijadhadh.2008.09.008.
[46] S. Ferraris, S. Yamaguchi, N. Barbani, M. Cazzola, C. Cristallini, M. Miola, E. Vernè, S. Spriano, Bioactive materials: in vitro investigation of different mechanisms of hydroxyapatite precipitation, Acta Biomater. 102 (2020) 468–480, https://doi.org/10.1016/j.actbio.2019.11.024.
[47] J.S. Stevens, A.C. De Luca, M. Pelendritis, G. Terenghi, S. Downes, S.L. M. Schroeder, Quantitative analysis of complex amino acids and RGD peptides by X-ray photoelectron spectroscopy (XPS), Surf. Interface Anal. 45 (2013) 1238–1246, https://doi.org/10.1002/sia.5261.
[48] K. Cai, J. Bossert, K.D. Jandt, Does the nanometre scale topography of titanium influence protein adsorption and cell proliferation? Colloids Surf. B Biointerfaces 49 (2006) 136–144, https://doi.org/10.1016/j.colsurfb.2006.02.016.
[49] D. Nečas, P. Klapetek, Gwyddion: an open-source software for SPM data analysis, Open Phys. 10 (2012) 181–188, https://doi.org/10.2478/s11534-011-0096-2.
[50] W. Norde, My voyage of discovery to proteins in flatland ...and beyond, Colloids Surf. B Biointerfaces 61 (2008) 1–9, https://doi.org/10.1016/j.colsurfb.2007.09.029.
[51] M. Miola, E. Verné, Bioactive and antibacterial glass powders doped with copper by ion-exchange in aqueous solutions, Materials 9 (2016) 1–16, https://doi.org/10.3390/ma9060405.
[52] L.H. Tjeng, M.B.J. Meinders, J. van Elp, J. Ghijsen, G.A. Sawatzky, R.L. Johnson, Electronic structure of Ag2O, Phys. Rev. B 41 (1990) 3190–3199, https://doi.org/10.1103/PhysRevB.41.3190.
[53] G. Schön, J. Tummavuori, B. Lindström, C.R. Enzell, C.R. Enzell, C.-G. Swahn, ESCA studies of Ag, Ag2O and AgO, Acta Chem. Scand. 27 (1973) 2623–2633, https://doi.org/10.3891/acta.chem.scand.27-2623.
[54] J.R. Jones, Review of bioactive glass: from Hench to hybrids, Acta Biomater. 9 (2013) 4457–4486, https://doi.org/10.1016/j.actbio.2012.08.023.
[55] S. Ferraris, F. Warkomicka, J. Barberi, A. Cochis, A.C. Scalia, S. Spriano, Contact guidance effect and prevention of microfouling on a beta titanium alloy surface structured by electron-beam technology, Nanomaterials 11 (2021), https://doi.org/10.3390/nano11061474.
[56] H. Lan, H. Liu, Y. Ye, Z. Yin, The role of surface properties on protein aggregation behavior in aqueous solution of different pH values, AAPS PharmSciTech 21 (2020) 1–13, https://doi.org/10.1208/s12249-020-01663-7.
[57] T. Kopac, K. Bozgeyik, Effect of surface area enhancement on the adsorption of bovine serum albumin onto titanium dioxide, Colloids Surf. B Biointerfaces 76 (2010) 265–271, https://doi.org/10.1016/j.colsurfb.2009.11.002.
[58] N. Miyake, T. Sato, Y. Maki, Effect of zeta potentials on bovine serum albumin adsorption to hydroxyapatite surfaces, Bull. Tokyo Dent. Coll. 54 (2013) 97–101, https://doi.org/10.2209/tdcpublication.54.97.
[59] T. Luxbacher, The Zeta Potential for Solid Surface Analysis, Anton Paar GmbH, 2014.
[60] F.M. Fowkes, D.W. Dwight, D.A. Cole, T.C. Huang, Acid-base properties of glass surfaces, J. Non-Cryst. Solids 120 (1990) 47–60, https://doi.org/10.1016/0022-3093(90)90190-W.
[61] A. Bismarck, A.R. Boccaccini, E. Egia-Ajuriagojeaskoa, D. Hülsenberg, T. Leutbecher, Surface characterization of glass fibers made from silicate waste: zeta-potential and contact angle measurements, J. Mater. Sci. 39 (2004) 401–412, https://doi.org/10.1023/B:JMSC.0000011493.26161.a6.
[62] S. Ferraris, S. Yamaguchi, N. Barbani, C. Cristallini, G. Gautier di Confiengo, J. Barberi, M. Cazzola, M. Miola, E. Vernè, S. Spriano, The mechanical and chemical stability of the interfaces in bioactive materials: the substrate-bioactive surface layer and hydroxyapatite-bioactive surface layer interfaces, Mater. Sci. Eng. C 116 (2020), 111238, https://doi.org/10.1016/j.msec.2020.111238.
[63] D. Guldiren, I. Erdem, S. Aydin, Influence of silver and potassium ion exchange on physical and mechanical properties of soda lime glass, J. Non-Cryst. Solids 441 (2016) 1–9, https://doi.org/10.1016/j.jnoncrysol.2016.03.007.
[64] W. Norde, Driving forces for protein adsorption at solid surfaces, Macromol. Symp. 103 (1996) 5–18, https://doi.org/10.1002/masy.19961030104.
[65] J. Lu, C. Yao, L. Yang, T.J. Webster, Decreased platelet adhesion and enhanced endothelial cell functions on nano and submicron-rough titanium stents, Tissue Eng. 18 (2012) 1389–1398, https://doi.org/10.1089/ten.tea.2011.0268.
[66] I. Firkowska-Boden, X. Zhang, K.D. Jandt, Controlling protein adsorption through nanostructured polymeric surfaces, Adv. Healthc. Mater. 7 (2018), https://doi.org/10.1002/adhm.201700995.
[67] Y.S. Hedberg, M.S. Killian, E. Blomberg, S. Virtanen, P. Schmuki, I. Odnevall Wallinder, Interaction of bovine serum albumin and lysozyme with stainless steel studied by time-of-flight secondary ion mass spectrometry and X-ray photoelectron spectroscopy, Langmuir 28 (2012) 16306–16317, https://doi.org/10.1021/la3039279.
[68] X.N. Hu, B.C. Yang, Conformation change of bovine serum albumin induced by bioactive titanium metals and its effects on cell behaviors, J. Biomed. Mater. Res., Part A 102 (2014) 1053–1062, https://doi.org/10.1002/jbm.a.34768.
[69] J. Barberi, L. Mandrile, L. Napione, A.M. Giovannozzi, A.M. Rossi, A. Vitale, S. Yamaguchi, S. Spriano, Albumin and fibronectin adsorption on treated titanium surfaces for osseointegration: an advanced investigation, Appl. Surf. Sci. 599 (2022), 154023, https://doi.org/10.1016/j.apsusc.2022.154023.
[70] C. Gruian, E. Vanea, S. Simon, V. Simon, FTIR and XPS studies of protein adsorption onto functionalized bioactive glass, Biochim. Biophys. Acta, Proteins Proteomics 1824 (2012) 873–881, https://doi.org/10.1016/j.bbapap.2012.04.008.
[71] R.N. Foster, E.T. Harrison, D.G. Castner, ToF-SIMS and XPS characterization of protein films adsorbed onto bare and sodium styrenesulfonate-grafted gold substrates, Langmuir 32 (2016) 3207–3216, https://doi.org/10.1021/acs.langmuir.5b04743.
[72] L. Varila, S. Fagerlund, T. Lehtonen, J. Tuominen, L. Hupa, Surface reactions of bioactive glasses in buffered solutions, J. Eur. Ceram. Soc. 32 (2012) 2757–2763, https://doi.org/10.1016/j.jeurceramsoc.2012.01.025.
[73] D.-N. Le, H.T. Nguyen-Truong, Analytical formula for the electron inelastic mean free path, J. Phys. Chem. C 125 (2021) 18946–18951, https://doi.org/10.1021/acs.jpcc.1c05212.
[74] V.I. Garmash, N.A. Djuzhev, E.P. Kirilenko, M.A. Makhiboroda, D.M. Migunov, Experimental determination of the energy dependence of electron inelastic mean free path in silicon oxide and silicon nitride, J. Surf. Investig. 10 (2016) 767–770, https://doi.org/10.1134/S1027451016040066.
[75] P.J. Cumpson, Estimation of inelastic mean free paths for polymers and other organic materials: use of quantitative structure-property relationships, Surf. Interface Anal. 31 (2001) 23–34, https://doi.org/10.1002/sia.948.
[76] Z. Tan, Y. Xia, M. Zhao, X. Liu, Electron stopping power and inelastic mean free path in amino acids and protein over the energy range of 20-20,000 eV, Radiat, Environ. Biophys. 45 (2006) 135–143, https://doi.org/10.1007/s00411-006-0049-0.
[77] L. Burgos-Asperilla, M.C. García-Alonso, M.L. Escudero, C. Alonso, Study of the interaction of inorganic and organic compounds of cell culture medium with a Ti surface, Acta Biomater. 6 (2010) 652–661, https://doi.org/10.1016/j.actbio.2009.06.019.
[78] G. Riccucci, M. Cazzola, S. Ferraris, V.A. Gobbo, M. Guaita, S. Spriano, Surface functionalization of Ti6Al4V with an extract of polyphenols from red grape pomace, Mater. Des. 206 (2021), 109776, https://doi.org/10.1016/j.matdes.2021.109776.
[79] A.V. Shchukarev, D.V. Korolkov, XPS study of group IA carbonates, Cent. Eur. J. Chem. 2 (2004) 347–362, https://doi.org/10.2478/BF02475578.
[80] A. Shchukarev, B.Ö. Malekzadeh, M. Ransjö, P. Tengvall, A. Westerlund, Surface characterization of insulin-coated Ti6Al4V medical implants conditioned in cell culture medium: an XPS study, J. Electron. Spectrosc. Relat. Phenom. 216 (2017) 33–38, https://doi.org/10.1016/j.elspec.2017.03.001.
[81] K. Siriwardana, A. Wang, M. Gadogbe, W.E. Collier, N.C. Fitzkee, D. Zhang, Studying the effects of cysteine residues on protein interactions with silver nanoparticles, J. Phys. Chem. C 119 (2015) 2910–2916, https://doi.org/10.1021/jp512440z.
[82] K. Skorstengaard, M.S. Jensen, P. Sahl, T.E. Petersen, S. Magnusson, Complete primary structure of bovine plasma fibronectin, Eur. J. Biochem. 161 (1986) 441–453, https://doi.org/10.1111/j.1432-1033.1986.tb10464.x.
[83] A. Cochis, J. Barberi, S. Ferraris, M. Miola, L. Rimondini, E. Vernè, S. Yamaguchi, S. Spriano, Competitive surface colonization of antibacterial and bioactive materials doped with strontium and/or silver ions, Nanomaterials 10 (2020) 120, https://doi.org/10.3390/nano10010120.
[84] A. Dolatshahi-Pirouz, T. Jensen, D.C. Kraft, M. Foss, P. Kingshott, J.L. Hansen, A. N. Larsen, J. Chevallier, F. Besenbacher, Fibronectin adsorption, cell adhesion, and proliferation on nanostructured tantalum surfaces, ACS Nano 4 (2010) 2874–2882, https://doi.org/10.1021/nn9017872.
[85] C.J. Wiedermann, Anti-inflammatory activity of albumin, Crit. Care Med. 35 (2007) 981–982, https://doi.org/10.1097/01.CCM.0000257234.87784.91.
[86] A.M. Negrescu, A. Cimpean, The state of the art and prospects for osteoimmunomodulatory biomaterials, Materials 14 (2021), https://doi.org/10.3390/ma14061357.
[87] J. Barberi, S. Ferraris, A.M. Giovannozzi, L. Mandrile, E. Piatti, A.M. Rossi, S. Spriano, Advanced characterization of albumin adsorption on a chemically treated surface for osseointegration: an innovative experimental approach, Mater. Des. 218 (2022), 110712, https://doi.org/10.1016/j.matdes.2022.110712.
[88] Y. Yan, H. Yang, Y. Su, L. Qiao, Albumin adsorption on CoCrMo alloy surfaces, Sci. Rep. 5 (2015) 1–10, https://doi.org/10.1038/srep18403.
[89] E. Rahimi, R. Offoiach, K. Baert, H. Terryn, M. Lekka, L. Fedrizzi, Role of phosphate, calcium species and hydrogen peroxide on albumin protein adsorption on surface oxide of Ti6Al4V alloy, Materialia 15 (2021), https://doi.org/10.1016/j.mtla.2020.100988.
[90] C.A. Scotchford, C.P. Gilmore, E. Cooper, G.J. Leggett, S. Downes, Protein adsorption and human osteoblast-like cell attachment and growth on alkylthiol on gold self-assembled monolayers, J. Biomed. Mater. Res. 59 (2002) 84–99, https://doi.org/10.1002/jbm.1220.
[91] P. Yu, X. Zhu, X. Wang, S. Wang, W. Li, G. Tan, Y. Zhang, C. Ning, Periodic nanoneedle and buffer zones constructed on a titanium surface promote osteogenic differentiation and bone calcification in vivo, Adv. Healthc. Mater. 5 (2016) 364–372, https://doi.org/10.1002/adhm.201500461.
[92] A. Barth, Infrared spectroscopy of proteins, Biochim. Biophys. Acta, Bioenerg. 1767 (2007) 1073–1101, https://doi.org/10.1016/j.bbabio.2007.06.004.
[93] L.A. Buchanan, A. El-Ghannam, Effect of bioactive glass crystallization on the conformation and bioactivity of adsorbed proteins, J. Biomed. Mater. Res., Part A 93 (2010) 537–546, https://doi.org/10.1002/jbm.a.32561.
[94] M. Jackson, H.H. Mantsch, The use and misuse of FTIR spectroscopy in the determination of protein structure, Crit. Rev. Biochem. Mol. Biol. 30 (1995) 95–120, https://doi.org/10.3109/10409239509085140.
[95] A. Gand, M. Tabuteau, C. Chat, G. Ladam, H. Atmani, P.R. Van Tassel, E. Pauthe, Fibronectin-based multilayer thin films, Colloids Surf. B Biointerfaces 156 (2017) 313–319, https://doi.org/10.1016/j.colsurfb.2017.05.023.

[96] M. Xiao, M. Biao, Y. Chen, M. Xie, B. Yang, Regulating the osteogenic function of rhBMP 2 by different titanium surface properties, J. Biomed. Mater. Res., Part A 104 (2016) 1882–1893, https://doi.org/10.1002/jbm.a.35719.

[97] Y. Li, Y. Bian, H. Qin, Y. Zhang, Z. Bian, Photocatalytic reduction behavior of hexavalent chromium on hydroxyl modified titanium dioxide, Appl. Catal. B Environ. 206 (2017) 293–299, https://doi.org/10.1016/j.apcatb.2017.01.044.

[98] K. Murayama, M. Tomida, Heat-induced secondary structure and conformation change of bovine serum albumin investigated by fourier transform infrared spectroscopy, Biochemistry 43 (2004) 11526–11532, https://doi.org/10.1021/bi0489154.

[99] L. Parisi, A. Toffoli, B. Ghezzi, B. Mozzoni, S. Lumetti, G.M. Macaluso, A glance on the role of fibronectin in controlling cell response at biomaterial interface, Jpn. Dent. Sci. Rev. 56 (2020) 50–55, https://doi.org/10.1016/j.jdsr.2019.11.002.

[100] A. Hamad, K.S. Khashan, A. Hadi, Silver nanoparticles and silver ions as potential antibacterial agents, J. Inorg. Organomet. Polym. Mater. 30 (2020) 4811–4828, https://doi.org/10.1007/s10904-020-01744-x.

[101] A.J. Raghavendra, N. Alsaleh, J.M. Brown, R. Podila, Charge-transfer interactions induce surface dependent conformational changes in apolipoprotein biocorona, Biointerphases 12 (2017), 02D402, https://doi.org/10.1116/1.4977064.

[102] I. Wierzbicka-Patynowski, J.E. Schwarzbauer, The ins and outs of fibronectin matrix assembly, J. Cell Sci. 116 (2003) 3269–3276, https://doi.org/10.1242/jcs.00670.

[103] D.J. Iuliano, S.S. Saavedra, G.A. Truskey, Effect of the conformation and orientation of adsorbed fibronectin on endothelial cell spreading and the strength of adhesion, J. Biomed. Mater. Res. 27 (1993) 1103–1113, https://doi.org/10.1002/jbm.820270816.

[104] N.E. Muzzio, M.A. Pasquale, X. Rios, O. Azzaroni, J. Llop, S.E. Moya, Adsorption and exchangeability of fibronectin and serum albumin protein corona on annealed polyelectrolyte multilayers and their consequences on cell adhesion, Adv. Mater. Interfac. 6 (2019), 1900008, https://doi.org/10.1002/admi.201900008.

[105] H.P. Felgueiras, S.D. Sommerfeld, N.S. Murthy, J. Kohn, V. Migonney, Poly(NaSS) functionalization modulates the conformation of fibronectin and collagen type i to enhance osteoblastic cell attachment onto Ti6Al4V, Langmuir 30 (2014) 9477–9483, https://doi.org/10.1021/la501862f.

[106] S. Bhattacharjee, DLS and zeta potential - what they are and what they are not? J. Contr. Release 235 (2016) 337–351, https://doi.org/10.1016/j.jconrel.2016.06.017.

[107] K. Kubiak-Ossowska, M. Cwieka, A. Kaczynska, B. Jachimska, P.A. Mulheran, Lysozyme adsorption at a silica surface using simulation and experiment: effects of pH on protein layer structure, Phys. Chem. Chem. Phys. 17 (2015) 24070–24077, https://doi.org/10.1039/c5cp03910j.

[108] T. Peters, All about Albumin, Elsevier, 1995, https://doi.org/10.1016/B978-0-12-552110-9.X5000-4.